

Design and Synthesis of Near-Infrared Absorbing Dyes for the Liquid Crystal Point-Diffraction Interferometer (LCPDI)

Introduction

Although considerable progress in achieving the goals of ICF has been made in recent years, considerable work still remains in improving direct-drive laser systems to the point where fuel ignition can occur. Because of difficulties in manufacturing large-aperture optical elements such as those used in OMEGA, these optics can add aberrations to each laser beam that can result in wavefront errors in the incident beams. Such wavefront errors can manifest themselves in unequal illumination of the target, which in turn reduces the uniformity of the energy being delivered by the laser. Although numerous diagnostic instruments are used on OMEGA to analyze beam-uniformity problems, a more effective method of measuring wavefront aberrations than is currently available is required. Shearing interferometry is currently used to analyze OMEGA beamlines, but the method suffers from (1) an inability to perform gradient measurements in more than two directions; (2) a low sensitivity to high-order phase errors; and (3) low spatial resolution. One approach taken to avoid these difficulties is to use a point-diffraction interferometric setup that relies on a liquid crystal (LC) electro-optical device as the primary modulation element. The fundamental design of this liquid crystal point-diffraction interferometer (LCPDI), as first introduced by Mercer and Creath,^{1,2} is similar to that of the general PDI design. In the LCPDI, however, an LC layer replaces the semitransparent filter of the conventional design, and the point used for diffraction (i.e., creation of the reference beam) is a microsphere embedded in the liquid crystal layer (Fig. 81.37). The incident beam is focused on the area of the cell that contains the microsphere, and optical interference occurs between the portions of the beam that pass through the glass microsphere and the liquid crystal fluid.

Phase shifting is accomplished by applying a voltage to the LC device, which undergoes a change in birefringence with applied voltage. A distinct advantage of the LCPDI is its common-path nature, i.e., both object and reference beams follow the same path as opposed to two different paths as in interferometers such as the Mach-Zehnder. This attribute makes the LCPDI less sensitive to environmental disturbances such

as mechanical vibration, temperature fluctuations, and air turbulence. It is also inherently phase shifting, allowing higher spatial sampling and generally more accurate wavefront characterization than other interferometric techniques. The single-path design also requires fewer optical elements than the Mach-Zehnder, thereby reducing size and cost of the instrument. Mercer, Rashidnia, and Creath³ have shown that for operation in the visible region the LCPDI is significantly more robust when compared with a phase-shifting Mach-Zehnder interferometer.³

Because the imaged area of the LCPDI device is substantially larger than the cross-sectional area of the microsphere, the portion of the beam that passes through the LC fluid must be attenuated to obtain sufficient contrast to analyze output images. In practice, this attenuation has been accomplished by adding a “guest” dye to the LC fluid “host” material used in the device. The LC host material is a commercial nematic LC

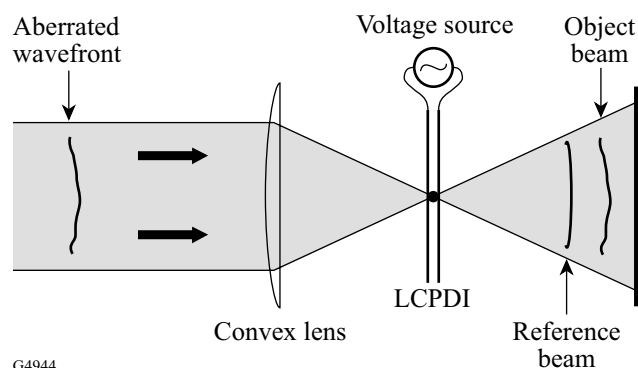


Figure 81.37 Schematic diagram of the liquid crystal point-diffraction interferometer (LCPDI). The laser beam is focused onto an area of the liquid crystal electro-optical device containing a glass or plastic sphere in the LC fluid gap. The portion of the beam passing through the microsphere functions as the reference arm of the interferometer. Application of an electric field to the birefringent LC material produces controlled molecular reorientation with subsequent generation of interference fringes. (Microsphere not drawn to scale.)

mixture of cyanobiphenyl and cyanoterphenyl components (Merck E7), which possesses a relatively high birefringence and positive dielectric anisotropy (Fig. 81.38).

For successful device operation, the guest dye must meet a number of important criteria:

- a strong absorbance maximum at or near the wavelength of incident laser radiation;
- high solubility in the liquid crystal host to maximize contrast and avoid long-term precipitation;
- excellent chemical and thermal stability; and
- low impact on the long-range molecular ordering in the LC host.

Two additional properties that would be highly desirable in dyes intended for LCPDI devices are (1) a low or nonexistent dichroism of the absorption band of interest so as to assure a constant attenuation with applied electric field, and (2) a liquid crystalline phase to allow larger amounts of the dye to be added without degrading the inherent molecular ordering of the host.

Although hundreds of dyes for visible-region LCPDI devices are commercially available, the selection of available dyes for the near IR is considerably more limited, and only a small subset of these absorb at the required 1054-nm wave-

length for operation in OMEGA. A further complication is that nearly all of these commercially available near-IR dyes are ionic or highly polar and, as such, show poor solubility in hydrocarbon-like liquid crystal hosts (0.01 to 0.05 wt%). One such example of this type of dye is shown in Fig. 81.39. The low solubility of these dyes essentially limits them to a maximum blocking extinction, or optical density (OD), in the LC host of <0.1, which is two decades less than required for producing acceptable fringe contrast for diagnostic purposes. The lack of a suitable near-IR dye candidate with sufficient LC host solubility dictated that a new dye or series of dyes be synthesized for the LCPDI device to meet its design goals.

Dye Selection and Design

The dye systems that were chosen for study are based on zerovalent transition metal dithiolene complexes,^{4,5} which are known to exhibit strong absorbance bands in the 600- to 1500-nm region of the spectrum and to be soluble in nonpolar organic solvents, depending on the dye's molecular structure. Our investigations focused on compounds using nickel as the central transition element (Fig. 81.40). Nickel dithiolenes are of special interest for this application because of their high solubility (up to 10 wt%) in liquid crystalline hosts⁶ and because the dyes themselves can possess liquid crystalline properties if appropriate terminal functional groups are selected.^{6,7} The latter is a distinct advantage because it would allow higher concentrations of the dye to be added to the liquid crystalline host without substantially reducing its degree of order.

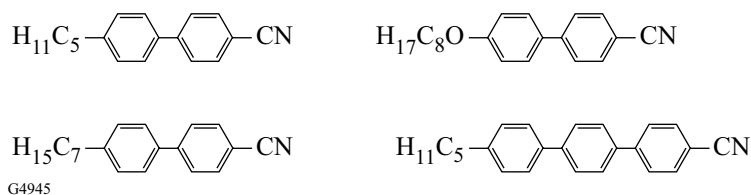


Figure 81.38

Composition of Merck E7, a high-birefringence nematic LC mixture with positive dielectric anisotropy used as the active host medium for the LCPDI device.

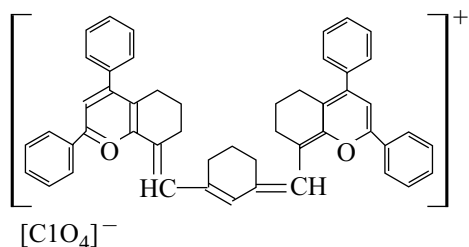


Figure 81.39

Molecular structure of a commercially available laser dye *Q*-switch 5 (Exciton, Inc). Because of their ionic and highly polar nature, nearly all laser dyes exhibit poor solubility in hydrocarbon-like liquid crystal host materials such as E7.

The strong near-infrared absorbance maxima observed in the nickel dithiolenes is a function of both extensive electron delocalization within the dithiolene ring system and interaction of this delocalized system with available d-orbitals on the

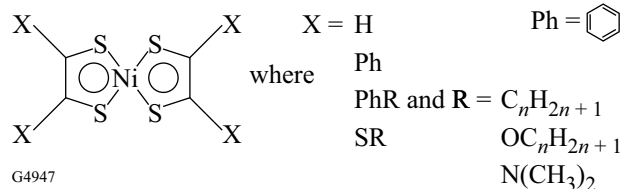


Figure 81.40

The molecular structure of transition metal dithiolenes with nickel as the central metal. The physical properties of the complex are determined by the nature of the terminal functional groups, designated as X, in the figure.

central metal.⁸ This interaction can be depicted both graphically and mathematically by using the linear combination of the atomic orbital–molecular orbital (LCAO–MO) theory. Here the atomic orbitals of the individual atoms are combined to form a series of lower-energy “bonding” and higher-energy “anti-bonding” molecular orbitals. Absorption of photons of sufficient energy results in promotion of electrons from occupied (bonding) molecular orbitals to unoccupied (anti-bonding) molecular orbitals. The lowest-energy transition, and thus the one that occurs at the longest wavelength, occurs between the highest occupied molecular orbital (HOMO) and the lowest unoccupied molecular orbital (LUMO) and is referred to as the bandgap. This HOMO/LUMO transition is responsible for the strong near-IR absorption in the nickel dithiolenes.^{4,8} Figures 81.41 and 81.42 show ground-state electronic-charge-distribution maps and HOMO/LUMO electron-density-

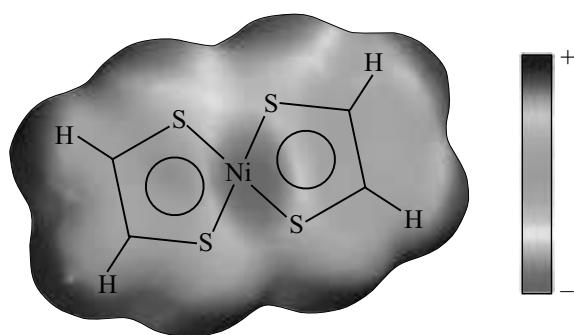


Figure 81.41

Ground-state charge-distribution map of the nickel dithiolene core. The shaded areas indicate electron-rich areas in the molecule.

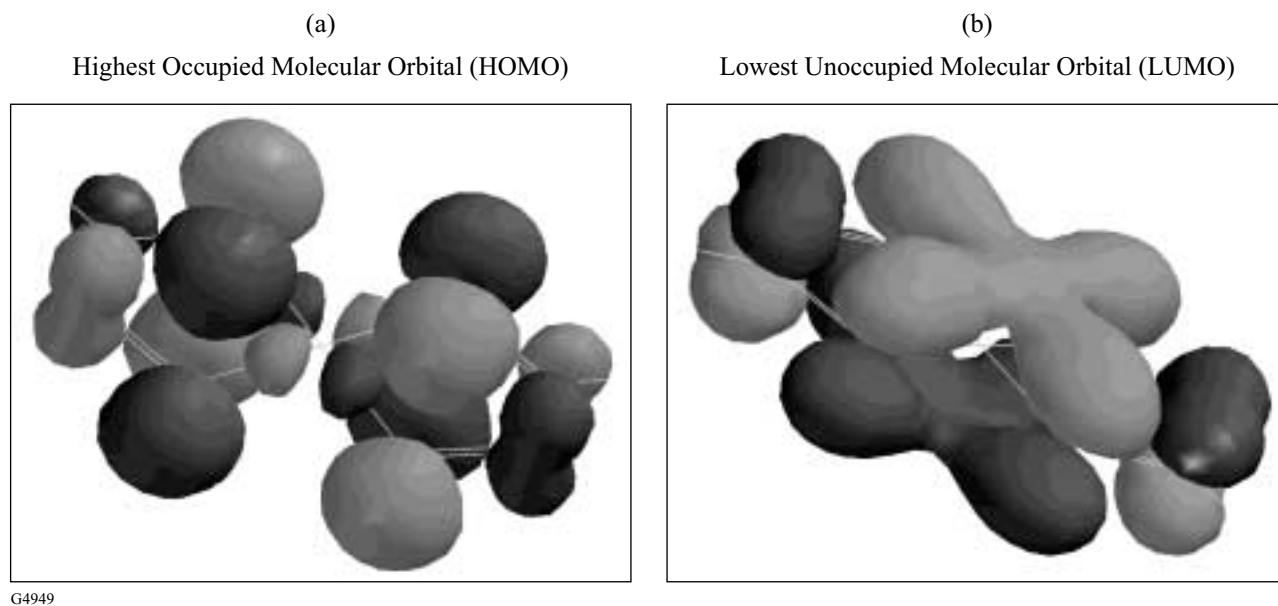


Figure 81.42

Electron-density probability maps of HOMO (left) and the LUMO (right) for the nickel dithiolene core.

probability maps, respectively, over the nickel dithiolenene core as generated by Spartan 5.0 computational chemistry software (Wavefunction, Inc.). The energy levels in electron volts for each molecular orbital can also be represented graphically, as shown in Fig. 81.43 for the nickel dithiolenene core of Fig. 81.41. The nature of the functional groups attached to the nickel dithiolenene core has a large effect on both the position of the electronic absorbance maximum and the solubility of the dye in the host matrix. Figure 81.44 compares the spectroscopic and solubility properties of two *para*-substituted nickel dithiolenenes that have been previously studied in liquid crystal host systems.⁶

Because the above two compounds represented nearly the sum total of literature data on the behavior of near-IR dyes in LC hosts, we chose to use these materials as the basis of our design and synthesis efforts. Our goal was to test different combinations of functional groups on the nickel dithiolenene core, both empirically and computationally, to observe their effect on both solubility and optical absorbance. To this end, we initiated the synthesis of a series of materials based on compound (a) in Fig. 81.44 with terminal alkyl and alkoxy groups

for initial studies of solubility and spectroscopic properties in the E7 LC host. In a parallel effort, we attempted to use computational chemistry methods to aid in predicting the appropriate functional group combinations that would yield materials with the desired solubility and spectroscopic parameters. These calculations were performed using the computational chemistry software packages Spartan 5.0 for molecular geometry optimization and Jaguar 3.5 (Schrödinger, Inc.) for solubility calculations.

Structural energy minimization calculations using semiempirical methods were undertaken using Spartan 5.0 prior to conducting the solubility calculations to ensure that the structural geometry of the compounds under evaluation was in its lowest-energy conformation. We chose the semiempirical approach because it can accurately predict equilibrium geometry using much less computing resources than *ab initio* and density functional methods and, when proper parameters for transition metals are applied, can also take into account contributions from bonding to d-orbitals. All calculations were conducted using a DEC AlphaServer running the Digital UNIX operating system.

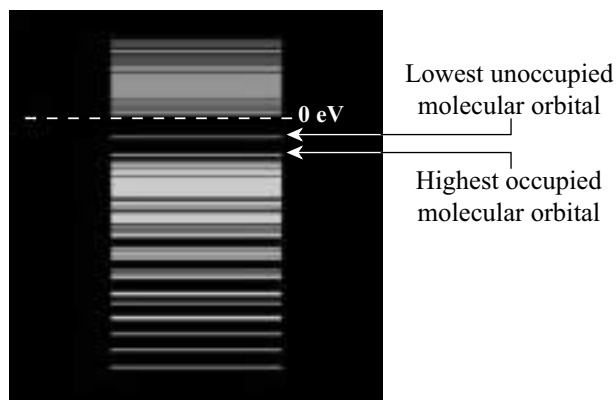
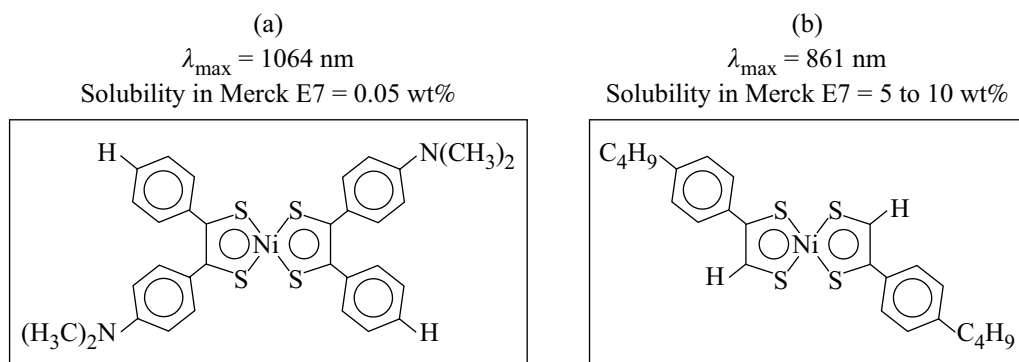


Figure 81.43

Energy levels for bonding (HOMO) and antibonding (LUMO) molecular orbitals in the nickel dithiolenene core shown in Fig. 81.41. The energy difference between the HOMO and LUMO is termed the bandgap and determines the portion of the spectrum (UV, visible, or near IR) where the electronic absorbance bands are observed.

G4950



G4951

Figure 81.44

Effect of molecular structure on solubility and spectroscopic properties of two substituted nickel dithiolenenes.

The solubility of a given solute in a solvent can be approximated by calculating its solvation energy and comparing this value with the bonding, or “reorganization,” energy. The solvation energy ΔG_{solv} is defined in Eq. (1) as⁹

$$\Delta G_{\text{solv}} = \Delta G_{\text{elec}} + \Delta G_{\text{cav}} + \Delta G_{\text{disp}} + \Delta G_{\text{vib}} + \Delta G_{\text{lib}} + \Delta G_{\text{other}}, \quad (1)$$

where ΔG_{solv} = solvation energy, ΔG_{elec} = electrostatic solute–solvent interaction, ΔG_{cav} = energy to form a solute shaped cavity, ΔG_{disp} = London and van der Waals interactions, ΔG_{vib} = change in vibrational energy due to damping, ΔG_{lib} = conversion of rotations and translations to librations, and ΔG_{other} = solvent enthalpic and entropic structure (PV term, etc.).

Although Spartan 5.0 has the ability to conduct geometry optimization in solution, it is not capable of dealing with d-orbitals in the solvation calculations. Because the metal d-orbitals play an extremely important role in determining the properties of the nickel dithiolenes, they must be taken into account in these calculations in order to obtain valid results. For these solubility calculations we instead opted to use Jaguar 3.5, a UNIX-based modeling package that does have this capability. Using the dielectric constant, molecular weight, and density of the solvent, Jaguar determines a “probe radius” parameter that is used to calculate the solvation energy.¹⁰

Solvated molecular systems are treated by Jaguar by means of a self-consistent reaction field method using its own Poisson–Boltzmann solver. The Poisson–Boltzmann equation [Eq. (2)]¹¹ sets the sum of the internal and external potentials equal to zero, allowing the program to solve for the elements of the solvation energy according to the three-dimensional grid mapped out by the equation using the finite difference method:

$$\nabla \cdot \epsilon(r) \nabla \phi(r) - \epsilon \kappa^2 \sinh[\phi(r)] + 4\pi q \rho^f(r) / kTf(\phi) = 0, \quad (2)$$

where ϵ = dielectric constant, q = proton charge, k = Boltzmann’s constant, T = absolute temperature, ρ^f = fixed charge density, $\phi(r)$ = dimensionless electrostatic potential in units of kT/q , r = position vector, and $\kappa^2 = 1/\lambda^2 = 8\pi q^2 I / \epsilon kT$, where λ = Debye length, and I = ionic strength of the bulk solution.

Because currently available software is incapable of conducting these calculations in solvent systems that are either (1) anisotropic in their physical properties or (2) mixtures of compounds, a direct calculation of dye solubility in the E7 nematic host mixture was not feasible. Our approach was instead to use single-component, *isotropic* solvents with molecular structures similar to that of the components in the E7 host so as to establish qualitative solubility trends with changes in terminal functional groups. Cyclohexane (a common organic solvent) and Merck CB-15 (an isotropic chiral cyanobiphenyl compound structurally similar to the components of E7) were chosen as the solvent host media for the calculations (Fig. 81.45). One difficulty encountered early in the solubility calculations was that the probe radius calculation assumes that the solvent host molecules are rigid and spherical. Although cyclohexane nicely fits this description (Fig. 81.45), CB-15 is a relatively long, cigar-shaped molecule and as such has a substantially larger probe radius value (3.647 Å, as calculated by Jaguar). Unfortunately, current limitations in the Jaguar software package restrict the maximum probe radius for the solvent host to a value of <3.1 Å, and we found it necessary to artificially limit the probe radius value for CB-15 to 2.8 Å in order for the calculations to proceed. The required reduction in probe radius has a minimal impact on the calculation, as the dielectric constant is the parameter that has the greatest influence on the calculated result. Table 81.V shows the calculated solvation energies obtained for compounds containing the nickel dithiolenes with a selected group of terminal functional groups as solutes in cyclohexane and CB-15. The value ΔG_{solv} can be used as a qualitative indicator of general solubility of the dye solutes in the same host, with a larger positive value generally indicating a greater solubility in the solvent host matrix. As shown in Table 81.V, the calculated ΔG_{solv} values imply that sulfur-containing substituents are expected to provide a substantial enhancement in solubility, with the greatest enhancement expected for alkylthio (-SR) terminal groups bonded directly to the nickel dithiolenes core.

Dye Synthesis

The synthesis of the nickel dithiolenes dyes and their precursors were conducted using literature methods^{12–15} with some modifications. The structural identity of synthesized products was verified using UV-visible–near-IR spectrophotometry, Fourier transform infrared (FTIR) spectrometry, and nuclear magnetic resonance (NMR) spectrometry. Product purity was assessed by high-performance liquid chromatography (HPLC) and, for crystalline products, by melting point via hot-stage polarizing microscopy. Phase transitions were

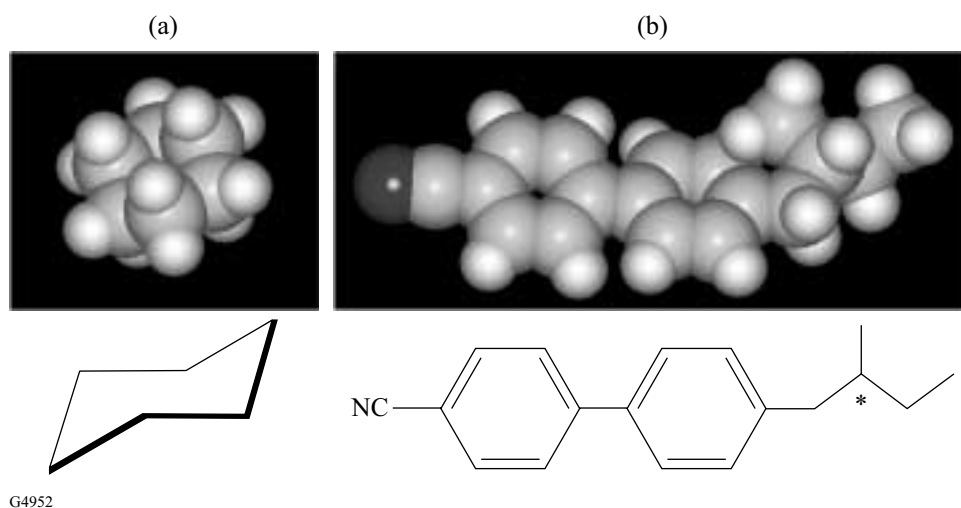


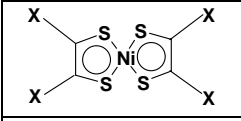
Figure 81.45

The solvent hosts used for the solubility calculations: (a) cyclohexane and (b) Merck CB-15. A space-filling graphical model of each solvent host is shown at the top of the figure, with the chemical structure drawn below. Note that the hydrogen atoms have been omitted in the structural formulas for clarity. The asterisk in the CB-15 structure indicates the presence of an asymmetric (chiral) carbon.

characterized by both differential scanning calorimetry (DSC) and hot-stage polarizing microscopy.

For materials with terminal substituents containing phenyl groups (-PhR and -PhOR), we used the method of Ohta *et al.*,¹² as shown in Fig. 81.46. Compounds with terminal alkythio substituents (-SR) were synthesized based on methods reported by Wainwright and Underhill,¹³ N. Svenstrup *et al.*,¹⁴ and A. Charlton *et al.*,¹⁵ which are shown in Fig. 81.47. Our modifications to the original published procedures afforded

Table 81.V: Results of solvation energy calculations on nickel dithiolene cores with various terminal functional groups in cyclohexane and CB-15 using Jaguar. A larger positive value indicates a greater solubility in the host matrix.

	ΔG_{solv} Cyclohexane (kcal/mole)	ΔG_{solv} Merck CB-15 (kcal/mole)
X = SC ₈ H ₁₇	6.9435	-7.6725
X = SC ₇ H ₁₅	6.2764	-7.7164
X = SC ₄ H ₉	3.9248	-7.7190
X = PhC ₄ H ₉	3.2985	-14.4373
X = PhN(CH ₃) ₂	0.0812	-17.4080
X = PhOC ₉ H ₁₉	5.2212	-21.6724
X = PhOC ₄ H ₉	0.9780	-21.6950

substantial improvements in yields of pure product in most cases. Table 81.VI gives the physical properties and yields of dyes synthesized by these two methods.

Solubility Studies

Prior to generation of a suitable mixture for use in the LCPDI device, the solubility limits of selected nickel dithiolene dyes in three host systems (cyclohexane, Merck CB-15, and Merck E7) were determined by means of a time-based sedimentation experiment. Samples of each dye chosen for study were prepared in the three host materials at select concentrations between 0.3 wt% to 1 wt%. Each dye was dissolved into 2 ml of each host by heating the host/dye mixture to an elevated temperature (40°C for cyclohexane and 100°C for CB-15 and E7) and stirring for several hours. Upon cooling, each sample was filtered through a 0.45- μm Teflon membrane filter to remove any insoluble material. All samples were checked periodically, both visually and by microscopic inspection at 100 \times magnification, for evidence of dye precipitation. For samples that showed precipitation at 0.3%, new mixtures at lower concentrations were prepared until a stable dye concentration was achieved. The results are shown in Table 81.VII, along with the ΔG_{solv} values previously calculated from Table 81.VI. Because such a large number of mixtures were required in the sedimentation experiment and only limited quantities of each dye were available, we were unable to determine an absolute upper solubility limit for each dye mixture combination. Experiments are currently underway to

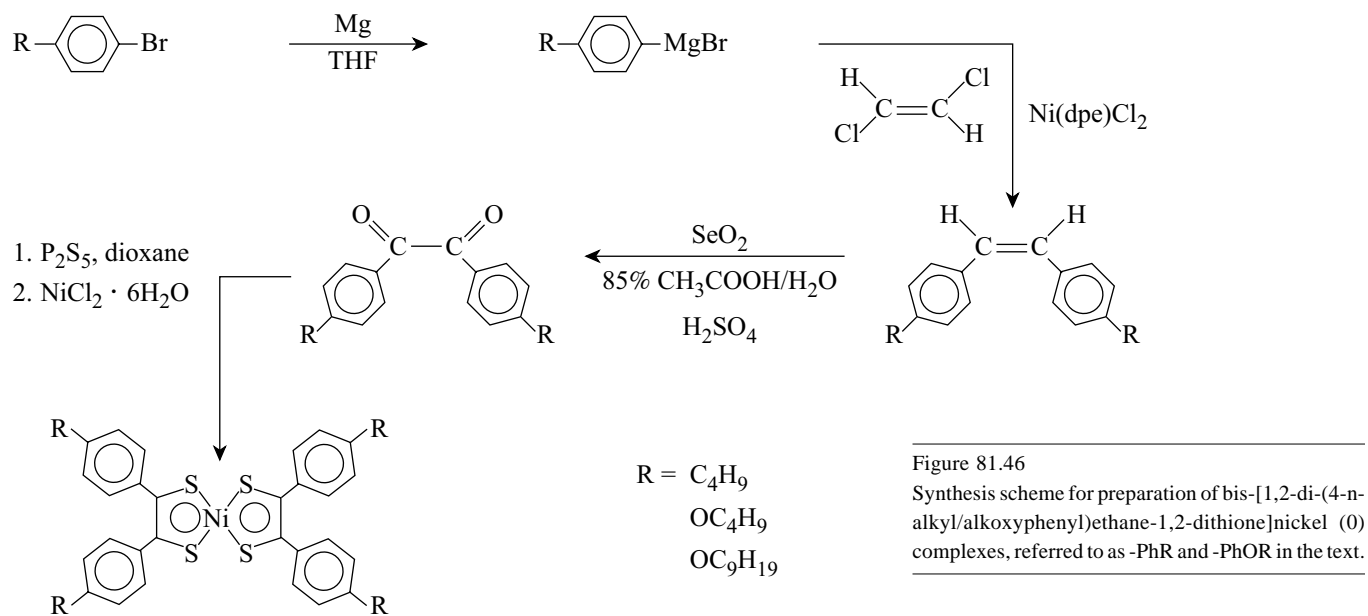


Figure 81.46
 Synthesis scheme for preparation of bis-[1,2-di-(4-n-alkyl/alkoxyphenyl)ethane-1,2-dithione]nickel (0) complexes, referred to as -PhR and -PhOR in the text.

G4953

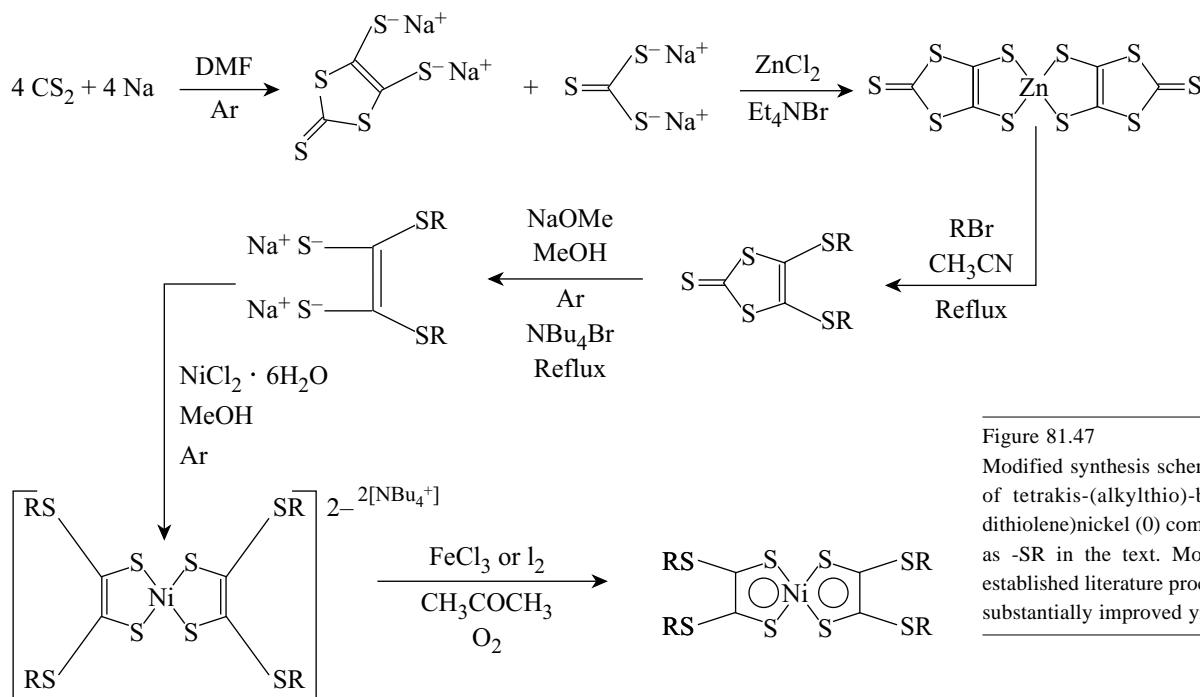


Figure 81.47
 Modified synthesis scheme for preparation of tetrakis-(alkylthio)-bis-(ethylene-1,2-dithiolene)nickel (0) complexes, referred to as -SR in the text. Modifications to the established literature procedures resulted in substantially improved yields of product.

G4954

more accurately determine the absolute solubility limit using only one supersaturated mixture for each dye/host pair by employing near-IR spectroscopic techniques.

A review of Tables 81.VI and 81.VII shows that there are substantial differences not only in the solubility of each dye in the different hosts but also in the position of its λ_{\max} as the host matrix is changed. In general, a 20- to 47-nm bathochromic

(red) shift is observed for these dyes in the anisotropic, ordered LC host as compared to an isotropic host such as acetone or cyclohexane.⁶ With regard to solubility, the experimental solubility data for the nickel dithiolenes in cyclohexane and CB-15 shows a substantial improvement in solubility when terminal -PhOR substituents are replaced with -SR groups, as was predicted by the computational modeling. This trend is also observed, but to a somewhat lesser degree, in the anisotropic

Table 81.VI: Properties of the substituted nickel dithiolenes synthesized for study as dye “guest” dopants for the LCPDI.

Terminal Group	Yield (%)		Melting point (°C)	λ_{\max} , acetone (nm)	Purity %
	Observed	Literature			
-PhC ₄ H ₉	51	N.R.	228.3–230.6	870	99.4
-PhOC ₄ H ₉	60	59	246.3–248.7	910	94.0
-PhOC ₉ H ₁₉	53	57	184.3–189.1	912	90.0
-SC ₄ H ₉	68	15	101	1002	99.3
-SC ₅ H ₁₁	64	15	95–98	1002	98.8
-SC ₆ H ₁₃	27	20	68.5–71.1	1002	98.1
-SC ₇ H ₁₅	41	27	81.5	1002	99.2
-SC ₈ H ₁₇	56	31	73	1002	99.3
-SC ₉ H ₁₉	29	30	80.4–81.2	1002	98.9
-SC ₁₀ H ₂₁	11	25	69.4–70.3	1002	96.5

N.R. = not reported

Table 81.VII: Comparison of calculated solvation energies and experimentally determined solubility limits of nickel dithiolenes in three host systems. For some dye mixture combinations, an absolute upper solubility limit has not been determined due to limited dye quantities.

Terminal (X) group	λ_{\max} in E7 (nm)	Cyclohexane		CB-15		Merck E7
		Solubility limit (wt%)	ΔG_{solv} (kcal/mole)	Solubility limit (wt%)	ΔG_{solv} (kcal/mole)	Solubility limit (wt%)
-SC ₈ H ₁₇	1020	≥0.5%	6.9435	≥1.0%	-7.6725	≤0.5%
-SC ₇ H ₁₅	1020	≥0.5%	6.2764	≤1.0%	-7.7164	≤0.5%
-SC ₄ H ₉	1020	≤0.5%	3.9248	≤1.0%	-7.7190	≤0.5%
-PhC ₄ H ₉	910	≤0.05%	3.2985	≤0.5%	-14.4373	≥0.3%
-PhN(CH ₃) ₂	1056	<0.5%	0.0812	≤0.5%	-17.4080	<0.1%
-PhOC ₉ H ₁₉	970	≤0.025%	5.2212	≤0.3%	-21.6724	<0.3%
-PhOC ₄ H ₉	970	<0.001%	0.9780	≤0.3%	-21.6950	≤0.3%

< = substantial precipitation at indicated value

≤ = marginal precipitation at indicated value

≥ = no precipitation at indicated value; actual upper solubility limit not determined

E7 LC host mixture intended for use in the LCPDI. The -SR materials will provide a larger blocking extinction at the same solution concentration than will their -PhOR counterparts since the λ_{max} of the -SR compounds in E7 is 70 to 110 nm closer to the 1054-nm operational wavelength of OMEGA than is the λ_{max} of the -PhOR substituted materials. The commercial dye with -PhN(CH₃)₂ substituents, although its λ_{max} is closest to 1054 nm and is nearly as soluble as the other dyes in cyclohexane and CB-15, displays the lowest solubility of the group in the E7 host.

Because no single dye has sufficient solubility in the E7 host to achieve the required OD of 1.8 to 2, it became necessary to use a mixture of several dyes to increase the total dye concentration past the general solubility limit of 0.3%–0.5% for each dye component.

LCPDI Guest–Host Mixtures

Multicomponent mixtures of various dyes from Table 81.VII were formulated and evaluated for their performance characteristics with regard to optical absorbance capability and stability in the E7 host LC fluid. Table 81.VIII gives the composition of these mixtures. The dye mixtures were prepared in the same manner as described earlier in the solubility experiments. LCPDI test cells were assembled from glass substrates bearing a 500-Å, transparent, conductive indium tin oxide (ITO) coating. The ITO surfaces were spin coated with a polyimide alignment coating, which, after baking and buffing, served as an alignment layer for the guest–host LC mixture. Glass spheres (25- μm diam) were deposited onto the coated, buffed surface of one substrate, and a second coated, buffed substrate was placed on top of the spheres with its rub direction anti-parallel

to the bottom substrate to define a 25- μm gap. The substrates were bonded together using Master Bond UV15-7TK1A UV curable epoxy, and the cells were filled with the LCPDI guest–host mixture by capillary action. Absorbance spectra of the devices were determined using a Perkin-Elmer Lambda 9 UV-VIS-NIR spectrophotometer with the incident beam polarized parallel to the cell alignment axis. Figure 81.48 compares the optical properties of the three mixtures. As is evident from Fig. 81.48, the mixture containing six -SR substituted dyes and one commercial -PhN(CH₃)₂ dye achieves the desired OD requirements for the LCPDI.

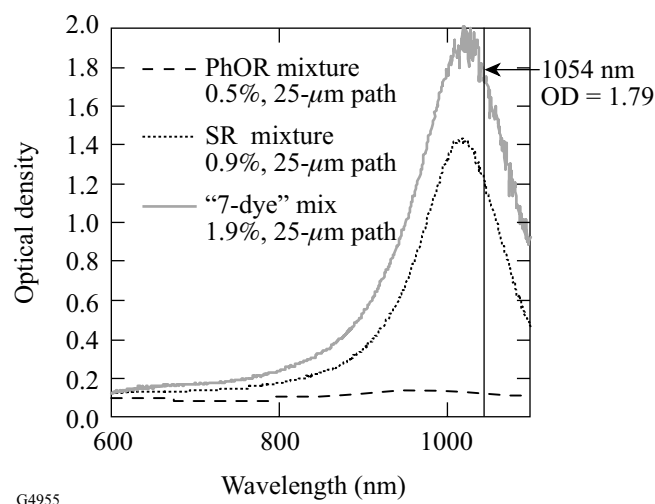


Figure 81.48 Optical-density data on three guest-host dye mixtures for the LCPDI. The measurements were made with the cell alignment axis parallel to the polarized incident beam of the spectrophotometer.

Table 81.VIII: Composition of three dye mixtures formulated for optical density (OD) evaluation in LCPDI test cells.

-PhOR mix		-SR mix		"7-dye" mix	
-PhOC ₄ H ₉	0.25%	-SC ₄ H ₉	0.3%	-SC ₄ H ₉	0.3%
-PhOC ₉ H ₁₉	0.25%	-SC ₇ H ₁₅	0.3%	-SC ₅ H ₁₁	0.3%
Total	0.5%	-SC ₈ H ₁₇	0.3%	-SC ₇ H ₁₅	0.3%
		Total	0.9%	-SC ₈ H ₁₇	0.3%
				-SC ₉ H ₁₉	0.3%
				-SC ₁₀ H ₂₁	0.3%
				-PhN(CH ₃) ₂	0.1%
				Total	1.9%

To date, there has been no evidence of crystallization or phase separation of dye components in this mixture after storage periods of several months, either in the bulk mixtures or in fabricated devices. In most-recent developments, a dye mixture containing a new nickel dithiolene compound that is a *liquid* at room temperature as an eighth dye component is being evaluated in an LCPDI device for its performance in the near IR. Devices containing this new mixture have displayed OD values of 2.77 and 1.85 for a 25- μm and 15- μm path length, respectively. The substantial improvement in OD afforded by this new compound now opens the possibility of fabricating thinner LCPDI devices that will exhibit improved contrast, reduced scattering losses, and faster electro-optic temporal response over previous-generation, near-IR devices.

Summary

The LCPDI device has exceptional potential for use in OMEGA due to a number of important attributes. Its inherently phase-shifting nature allows higher spatial sampling and generally more-accurate wavefront characterization than other interferometric techniques, while the single-path design requires fewer optical elements than other types of interferometers, thereby reducing size and cost requirements. The compact and “solid-state” nature of the device provides additional benefits in the form of reduced sensitivity to environmental disturbances such as mechanical vibration, temperature fluctuations, and air turbulence. The largest single obstacle to deployment of the LCPDI in OMEGA has been the availability of a near-IR dye with sufficient LC host solubility; chemical, thermal, and optical stability; and electronic absorbance properties to produce devices capable of sufficient contrast for output image analysis. Here, we have shown that, through selection of appropriate functional groups, zerovalent transition metal dithiolenes can be designed and synthesized that will allow the LCPDI to realize its design goals for deployment in OMEGA.

Although present computational chemistry methods and software are somewhat limited in scope for organometallic compounds, they can still provide useful qualitative guidance in the design and development of new dye compounds with solubility and optical absorbance requirements tailored to a specific host material. Using this approach, we demonstrated

both theoretically and experimentally that sulfur-containing alkyl terminal groups are superior to alkoxy, alkylphenyl, and alkoxyphenyl substituents both in enhancing the solubility of the nickel dithiolene core in the host medium and in optimizing the location of the dye λ_{max} for maximum absorbance efficiency. Employing a mixture of dyes rather than just a single-dye substance was shown to have two benefits: (1) a larger overall host dye concentration allows construction of thinner LCPDI devices with better performance characteristics, and (2) thermodynamic stability of the guest–host mixture is substantially enhanced since the relatively low concentration of each dye component reduces the risk of long-term dye precipitation from the host.

In addition to the pending evaluation of the capabilities of current near-IR LCPDI devices, experiments are also underway to more accurately determine the solubility limit of the dyes by spectroscopic techniques and to further refine the dye mixture composition so as to achieve additional gains in OD without sacrificing mixture stability. Our recent modeling efforts have generated a library of over 40 new transition metal dithiolene compounds that await further synthesis efforts to evaluate their potential as dye candidates for the LCPDI as well as for other near-IR LC device applications in optical communications and sensor protection.

ACKNOWLEDGMENT

The authors gratefully acknowledge the contributions of the following individuals and organizations: Dr. Julie R. Wright (Schroedinger, Inc.); Dr. W. Thomas Pollard (Schroedinger, Inc.); Dr. Wayne Huang (Wavefunction, Inc.); and Dr. Ansgar W. Schmid (LLE) for guidance and helpful discussions regarding computational chemistry methods and applications; Prof. Ulrich Muller-Westerhoff (Department of Chemistry, University of Connecticut) and Prof. Alan E. Underhill (Department of Chemistry, University of Wales) for helpful discussions on transition metal dithiolene syntheses; Irene Lippa (LLE) for determination of dye solubilities in host systems; Malia Moore, Awista Ayub, Scott Kinsella, and Kendra Bussey (LLE) for assistance in synthesis of metal complexes and precursors; and Tanya Kosci, Nathan Bickel, Ryan Brecker, and Markar Naradikian (LLE) for construction and characterization of the LCPDI devices. This work was supported by the U.S. Department of Energy Office of Inertial Confinement Fusion under Cooperative Agreement No. DE-FC03-92SF19460, the University of Rochester, and the New York State Energy Research and Development Authority. The support of DOE does not constitute an endorsement by DOE of the views expressed in this article.

REFERENCES

1. C. R. Mercer and K. Creath, *Opt. Lett.* **19**, 916 (1994).
2. C. R. Mercer and K. Creath, *Appl. Opt.* **35**, 1633 (1996).
3. C. R. Mercer, N. Rashidnia, and K. Creath, *Exp. Fluids* **21**, 11 (1996).
4. U. T. Mueller-Westerhoff, B. Vance, and D. I. Yoon, *Tetrahedron* **47**, 909 (1991).
5. P. Espinet *et al.*, *Coord. Chem. Rev.* **117**, 215 (1992).
6. K. L. Marshall and S. D. Jacobs, *Mol. Cryst. Liq. Cryst.* **159**, 181 (1988).
7. U. T. Mueller-Westerhoff *et al.*, *Mol. Cryst. Liq. Cryst. Lett.* **56**, 249 (1980).
8. U. T. Mueller-Westerhoff and B. Vance, in *Comprehensive Coordination Chemistry: The Synthesis, Reactions, Properties, and Applications of Coordination Compounds*, 1st ed. (Pergamon Press, Oxford, England, 1987), Vol. 2, pp. 595–631.
9. M. Colvin, "Continuum Models of Solvation," Lawrence Livermore National Laboratory (2000), available on the Internet at <http://gutenberg.llnl.gov/~colvin/solvation/solv.html>.
10. B. Lee and F. M. Richards, *J. Mol. Biol.* **55**, 379 (1971).
11. B. Honig, K. Sharp, and A. S. Yang, *J. Phys. Chem.* **97**, 1101 (1993).
12. K. Ohta *et al.*, *Mol. Cryst. Liq. Cryst.* **147**, 15 (1987).
13. C. E. A. Wainwright and A. E. Underhill, *Mol. Cryst. Liq. Cryst.* **234**, 193 (1993).
14. N. Svenstrup *et al.*, *Synthesis* **8**, 809 (1994).
15. A. Charlton *et al.*, *J. Mater. Chem.* **4**, 1861 (1994).

